# Classification and Quantification of Neuronal Fiber Pathways Using Diffusion Tensor MRI

Zhaohua Ding,* John C. Gore, and Adam W. Anderson

**Quantitative characterization of neuronal fiber pathways in vivo is of significant neurological and clinical interest. Using the capability of MR diffusion tensor imaging to determine the local orientations of neuronal fibers, novel algorithms were developed to bundle neuronal fiber pathways reconstructed in vivo with diffusion tensor images and to quantify various physical and geometric properties of fiber bundles. The reliability of the algorithms was examined with reproducibility tests. Illustrative results show that consistent physical and geometric measurements of novel properties of neuronal tissue can be obtained, which offer considerable potential for the quantitative study of fiber pathways in vivo. Magn Reson Med 49:716–721, 2003.**


**Key words: diffusion tensor imaging; fiber bundling; bundle properties**

Determination of neuronal fiber pathways in vivo is of significant neurological and clinical interest. For example, a precise knowledge of neuronal fiber connections can be used to better interpret functional relationships between different brain regions. Quantification of physical and geometric properties of neuronal fibers in vivo, along with their changes with time, can provide valuable insight into the progression of brain disease, while visualization of neuronal fiber pathways can assist the analysis of fiber connectivity and potentially guide brain surgery.

Determination of neuronal pathways in vivo becomes feasible with the advent of diffusion tensor imaging (DTI) using MR. DTI has proven to be effective for measuring the incoherent motions of water molecules. The directional dependence of water diffusion rates can be closely related to the structural anisotropy of the medium; DTI can thus be used to infer the organization and orientation of tissue components (1–5). In fact, the development of this technique has recently triggered considerable interest in noninvasively determining the neuronal connections provided by fiber pathways in the brain (6–11).

Most recent studies have focused on developing working algorithms to reconstruct neuronal fiber pathways using DTI. To date there has been little research in further processing of reconstructed fiber pathways, such as classifying fibers as members of distinct anatomical structures and quantitative characterization of these pathways. Motivated by its considerable potential in neurological studies and clinical applications, we have developed computer algorithms to bundle reconstructed fibers pathways into natural groups and quantify physical and geometric properties of the constructed fiber bundles. In the following, the relationship of diffusion tensor and fiber orientation is first briefly reviewed. Then a novel algorithm for bundling reconstructed fiber pathways is presented. Finally, the quantification of physical and geometric properties of fiber bundles is described, followed by illustrative results that demonstrate the reliability of the algorithms.

## METHODS

### Diffusion Tensor Imaging

The diffusion tensor is a matrix of coefficients describing the diffusion of water molecules:

$$\mathbf{D} = \begin{vmatrix} c_{11} & c_{12} & c_{13} \\ c_{12} & c_{22} & c_{23} \\ c_{13} & c_{23} & c_{33} \end{vmatrix}. \quad [1]$$

Diagonalization of **D** gives three pairs of eigenvalues and eigenvectors ($\lambda_i$ and $\mathbf{V}_i$, i = 1, 2, 3). Since molecular diffusion is hindered by encounters with cell membranes and cytoskeletal structures, the water diffusion rate parallel to a fiber is higher than perpendicular to it (1,12). The eigenvector corresponding to the largest eigenvalue is therefore parallel to the local tangent of a fiber.

The diffusion tensor is measured by sensitizing the MR signal intensity to the random motion of water (13). In our experiment, 3D diffusion tensor data were acquired with a 1.5 T, GE (General Electric, Milwaukee, WI) Signa LX magnetic resonance scanner, using a pulsed gradient spin echo pulse sequence. To minimize motion artifacts and reduce scanning time, single shot echo-planar imaging was used. A volume of $20 \times 20 \times 9$ cm$^3$ was scanned which generated a dataset of $64 \times 64 \times 18$ voxels for each case. For each voxel, seven measurements were made: one with no diffusion weighting and six with diffusion sensitization along noncolinear directions. The six independent coefficients of the diffusion tensor matrix were calculated using multivariate linear regression. To improve the signal-to-noise ratio of diffusion tensor images, four to eight repeated scans were performed on each subject. The final diffusion tensor matrix was calculated from the arithmetic mean of the DTI measurements.

### Bundling of Neuronal Fiber Pathways

Neuronal fiber pathways were reconstructed from 3D diffusion tensor imaging data acquired as above. The method employed is similar to that used in Ref. 8 and briefly summarized as follows: first, a 2D region which includes the fiber fascicles of interest is specified. Inside the 2D

Department of Diagnostic Radiology, Yale University School of Medicine, New Haven, Connecticut.

*Correspondence to: Zhaohua Ding, Vanderbilt University Institute of Imaging Science, 1161 21st Avenue South, MCN CCC-1118, Nashville, TN 37232-2675. E-mail: zhaohua.ding@vanderbilt.edu

Received 27 July 2001; revised 10 October 2002; accepted 14 November 2002.

DOI 10.1002/mrm.10415
Published online in Wiley InterScience (www.interscience.wiley.com).

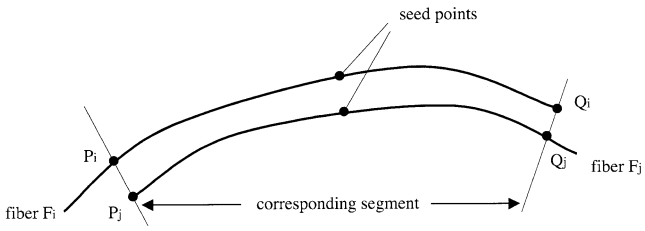


FIG. 1. Definition of corresponding segment. A corresponding segment is a portion of one fiber that has point-wise correspondence to a portion of another fiber (and vice versa). In this figure, $P_iQ_i$ of $F_i$ is the corresponding segment to $P_jQ_j$ of $F_j$.

region, a regular grid of closely spaced seed points is defined. A fiber pathway is then reconstructed for each of the seed points by sequentially following the direction of the eigenvector associated with the largest eigenvalue.

Fiber pathways connecting the same functional regions of the brain form a natural anatomical group (bundle). Fibers in the same bundle are usually clustered in 3D space, are approximately parallel to each other, and constitute a distinct structure from other fiber bundles. The process of fiber bundling is to partition a set of fiber pathways into different natural bundles.

Fiber bundling is a typical clustering problem. In cluster analysis, partitioning of a dataset into natural clusters can be achieved hierarchically or nonhierarchically. Hierarchical methods include divisive and agglomerative approaches (14). Divisive approaches involve splitting the whole dataset successively until a stop criterion is reached, while agglomerative approaches operate in the opposite direction. In this study, we employ a "K most-similar-fibers algorithm" to partition a set of fibers automatically into different natural bundles. This algorithm is similar to the "K nearest-neighbors algorithm" (15), which is in the category of hierarchical, agglomerative methods.

The process of fiber bundling begins with a definition of a similarity measure between a pair of fibers. First, we introduce the concept of a *corresponding segment*, which is loosely defined as the portion of a fiber ($F_i$) that has point-wise correspondence to a portion of another fiber ($F_j$), as illustrated in Fig. 1 (loosely speaking, these are the "overlapping" parts of the fibers). In this figure, segment $P_iQ_i$ of fiber $F_i$ is the corresponding segment to the segment $P_jQ_j$ of fiber $F_j$, and vice versa. A corresponding segment ratio is then defined as the ratio of the length of the corresponding segment to the overall length of the pair of fibers:

$$R_{cs} = \frac{L_{cs}}{L_i + L_j - L_{cs}}. \qquad [2]$$

Where $L_{cs}$ is the length of the corresponding segment; $L_i$ and $L_j$ are the length of $F_i$ and $F_j$, respectively. The corresponding segment ratio takes values between 0 (no overlap) and 1 (each fiber completely overlaps the other).

Measuring similarity between a pair of arbitrary spatial curves is a nontrivial problem. A major difficulty is to determine their corresponding segment. Our fiber data, however, have a convenient feature that facilitates the calculation of similarity. In our construction, all fiber pathways pass through the 2D plane that contains the seed points. Hence, the corresponding segment of a pair of fibers can be determined by searching the shorter end along both directions from the seed point. As shown in Fig. 1, the corresponding segment is spanned by $P_i$ and $Q_j$, the short end from the seed point along each direction, respectively.

Given a pair of fibers $F_i$ and $F_j$ that have corresponding segment $P_iQ_i$ and $P_jQ_j$, a mean Euclidean distance $D$ is measured over $P_iQ_i$ and $P_jQ_j$ (defined as average point-by-point distance between $P_iQ_i$ and $P_jQ_j$). The mean Euclidean distance $D$ is an indicator of shape similarity and location closeness of a pair of fibers. When two fibers are similar in shape and close in location (shown in Fig. 2a), the mean Euclidean distance $D$ is small; when the distance between a pair of fibers is large, or their shapes are different, $D$ is large (shown in Fig. 2b–d).

Two fibers are considered similar when they have comparable length, similar shape, and are separated by a small distance. The length comparability is measured by the corresponding ratio $R_{cs}$. The shape similarity and location closeness are indicated by the mean Euclidean distance $D$. Therefore, the similarity between a pair of fibers $F_i$ and $F_j$ can be defined in terms of the corresponding segment ratio $R_{cs}$ and the mean Euclidean distance $D$ as follows:

$$S_{ij} = R_{cs} \cdot \exp(-D/C). \qquad [3]$$

Where $R_{cs}$ is the corresponding segment ratio; $D$ is the mean Euclidean distance between corresponding segments of $F_i$ and $F_j$; and C is the coefficient for $D$.

Similarity defined as such is 1.0 when $F_i$ and $F_j$ are identical. It gets smaller when the corresponding segment ratio decreases, or the mean Euclidean distance $D$ increases. The coefficient C regulates a trade-off between the mean Euclidean distance $D$ and the corresponding segment ratio $R_{cs}$. When C is large, $D$ carries relatively less weighting in the calculation of similarity, or vice versa. In this study, C was chosen to be 1 voxel width.

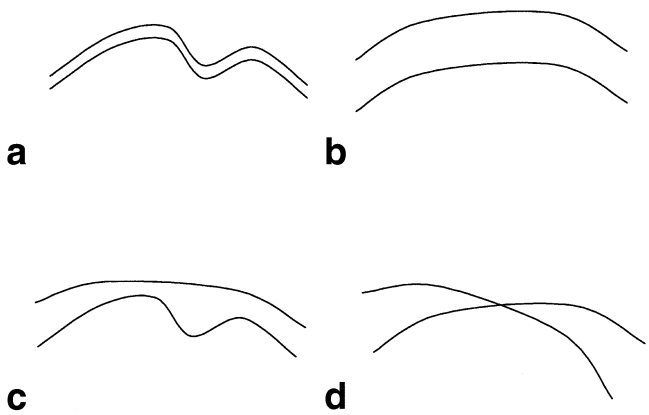


FIG. 2. The mean Euclidean distance $D$ indicates the shape similarity and location closeness of a pair of fibers. In **a**, two fibers are similar in shape and close in location and therefore $D$ is small. $D$ is large when the distance between them is large (**b**), or their shapes (**c**) or orientations are different (**d**).

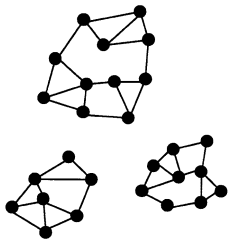

FIG. 3. Partitioning of a set of fibers into three connected components using a K most-similar-fibers algorithm. In this figure, each fiber is identified by its seed point. Similarity between fibers is represented by the distance between seed points. A fiber is connected to up to K most-similar-fibers in its neighborhood. Each connected component is a resulting fiber bundle.

With the definitions of corresponding segment ratio and similarity, the following steps are taken to bundle fibers:

1) For a fiber F, find eight fibers whose seed points are the neighbors of the seed point of F.
2) Calculate similarity $S$ between F and each of the eight neighboring fibers.
3) Threshold similarity such that any similarity value smaller than T ($0 \leq T \leq 1$) is set to 0.
4) Find up to K neighboring fibers whose nonzero similarity to F is greatest.
5) Group F with each of the fibers found in Ref. 4.

The above steps are repeated until all fibers are processed. This procedure results in partitioning the set of fibers into different grouped components, each of which constitutes a fiber bundle, as shown in Fig. 3.

In the bundling algorithm, two parameters are involved: the similarity threshold T and number of most-similar-fibers K. These parameters determine the characteristics of resulting fiber bundles. Specifically, the threshold T with an appropriate value precludes bridging of neighboring bundles, while the number of most-similar-fibers K decides the compactness of fiber bundles. In this study, the typical value for T is 0.4–0.8 and for K is 3 or 4.

### Quantification of Bundle Properties

Explicit bundling of a group of fiber pathways allows collective properties of an anatomical fiber bundle to be characterized. Quantities of potential value include physical parameters such as mean longitudinal and perpendicular diffusivity along the bundle length and geometric parameters such as curvature and torsion, all of which can be readily quantified. To calculate these parameters, the medial axis of a fiber bundle needs to be derived (see Fig. 4 for illustration). First, a cross-sectional plane that contains seed points of all the fibers in the bundle is identified (called the *seed plane*). The average of the coordinates of all seed points is taken as the centroid of the seed plane and the average of the path directions of all seed points is taken as the mean path direction at the seed plane. The next cross-sectional plane is determined to be the one which is perpendicular to the mean path direction and has distance d to the centroid. By repeating this process, we obtain a series of centroids, the sequential connection of which gives the medial axis of the fiber bundle.

The mean longitudinal diffusivity at a medial axial point is defined as the average of the largest eigenvalues of all fibers in the bundle measured at the location where the fibers intersect the cross-sectional plane and mean perpendicular diffusivity is the average of the geometric mean of the median and smallest eigenvalues.

Curvature and (helical) torsion along each bundle medial axis are calculated using a cubic polynomial fitting method (16): for a given point **P** on the medial axis, a window of 2N+1 points on the axis (and centered at **P**)is selected. These 2N+1 points are then fitted with a cubic polynomial curve by least square fitting to the $x$, $y$ and $z$ coordinates separately; i.e.:

$$x = a_0 + a_1\mu + a_2\mu^2 + a_3\mu^3 \quad [4]$$

$$y = b_0 + b_1\mu + b_2\mu^2 + b_3\mu^3 \quad [5]$$

$$z = c_0 + c_1\mu + c_2\mu^2 + c_3\mu^3 \quad [6]$$

where $\mu \in [0, 1]$.

First, second, and third derivatives of $x$, $y$, and $z$ with respect to $\mu$ are taken at $\mu = 0.5$; these derivatives are used to calculate curvature ($\kappa$) and torsion ($\tau$) according to the following equations (17):

$$\kappa = \left( \frac{(y'z'' - y''z')^2 + (z'x'' - z''x')^2 + (x'y'' - x''y')^2}{(x'^2 + y'^2 + z'^2)^3} \right)^{1/2} \quad [7]$$

$$\tau = \frac{\mathrm{abs}\begin{pmatrix} x' & y' & z' \\ x'' & y'' & z'' \\ x''' & y''' & z''' \end{pmatrix}}{(y'z'' - y''z')^2 + (z'x'' - z''x')^2 + (x'y'' - x''y')^2}. \quad [8]$$

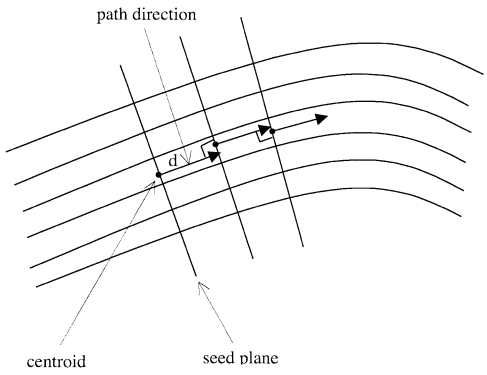


FIG. 4. Derivation of the medial axis of a fiber bundle. The seed plane which contains the seed points of all the fibers in the bundle is first identified. Each subsequent cross-sectional plane is perpendicular to the path direction of the previous plane and has a distance d to the previous centroid. The medial axis is a curve successively connecting all the centroids.

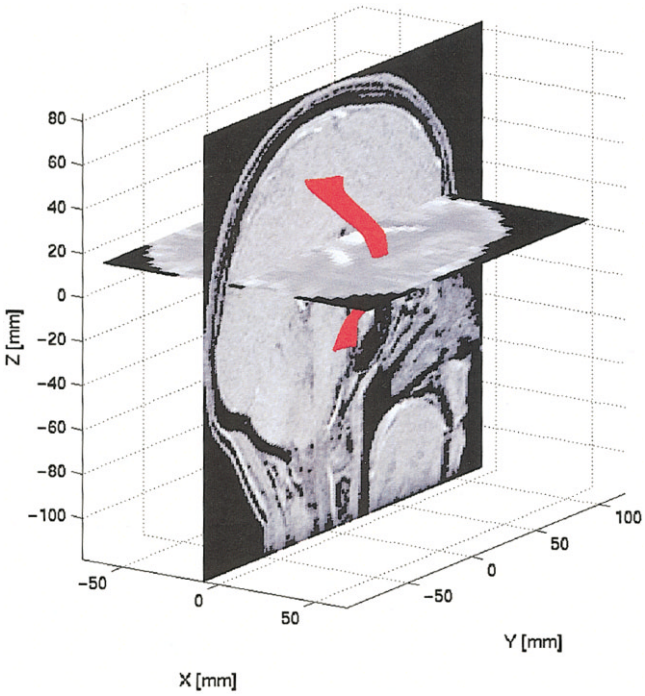


FIG. 5. Superposition of reconstructed fiber pathways onto anatomical images. These fiber pathways are reconstructed from seed points in a region that includes the right internal capsule.

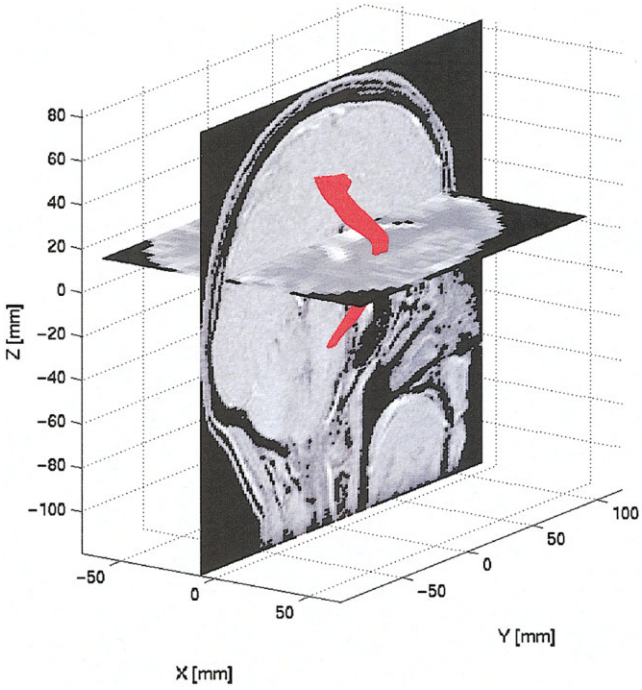


FIG. 7. Fiber pathways reconstructed with a second diffusion tensor dataset acquired from the same subject. Location and density of seed points are the same as in Fig. 5.

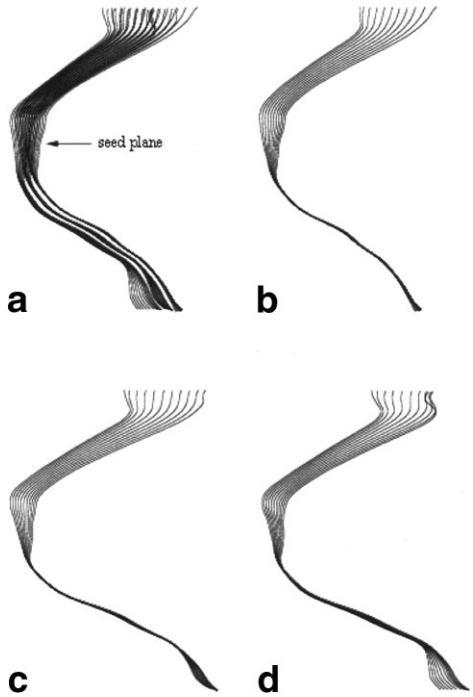


FIG. 6. **a:** The set of fiber pathways shown in Fig. 5. **b–d:** Three fiber bundles obtained from **a** with the bundling algorithm (T = 0.8, K = 3).

## RESULTS

Figure 5 shows a set of neuronal fiber pathways superimposed onto anatomical images. These pathways are reconstructed from seed points in a 2D region that contains the right internal capsule of a healthy volunteer. The size of the 2D region is $6 \times 6$ mm$^2$ and the density of seed points is $0.6 \times 0.6$ mm$^2$. The length of these bundles is approximately 140 mm. Figure 6 shows the set of fiber pathways in greater detail (Fig. 6a) and its three fiber bundles (Fig. 6b–d) formed with the bundling algorithm. The original fiber set contains more fiber pathways than shown in Figs. 5 and 6, but those forming small bundles are excluded from these figures for better demonstration of the bundling algorithm.

To test the reproducibility of the bundling algorithm, a second set of diffusion tensor data is obtained from the same subject. The data are acquired in an interleaved manner with the data used for Fig. 5, so that their imaging parameters are identical (acquisitions 1, 3, 5, and 7 were averaged to produce Fig. 5, and acquisitions 2, 4, 6, and 8 were analyzed to test reproducibility). Fiber pathways are reconstructed from seed points in the same region and at the same density. Similar bundling and quantification processes are performed on the reconstructed fiber pathways. The results from the second dataset are shown in Figs. 7 and 8. It can be seen that a similar set of fiber bundles to that shown in Fig. 6 is obtained, although they differ in some of the details. Similarity between corresponding fiber bundles is examined quantitatively by measuring mismatch between their medial axes. The mismatch is defined as the minimum distance of an axial point to the other axis, averaged over the axial length. The mismatches are found to be $1.25 \pm 0.51$ mm, $1.00 \pm 0.31$ mm, and $1.11 \pm 0.37$ mm for bundles b, c, and d, respectively.

The same approach is used to test the reproducibility of physical and geometric parameters of interest. First, the lengths of corresponding fiber bundles in Figs. 6 and 8 are matched respectively; then, mean parallel and perpendic-

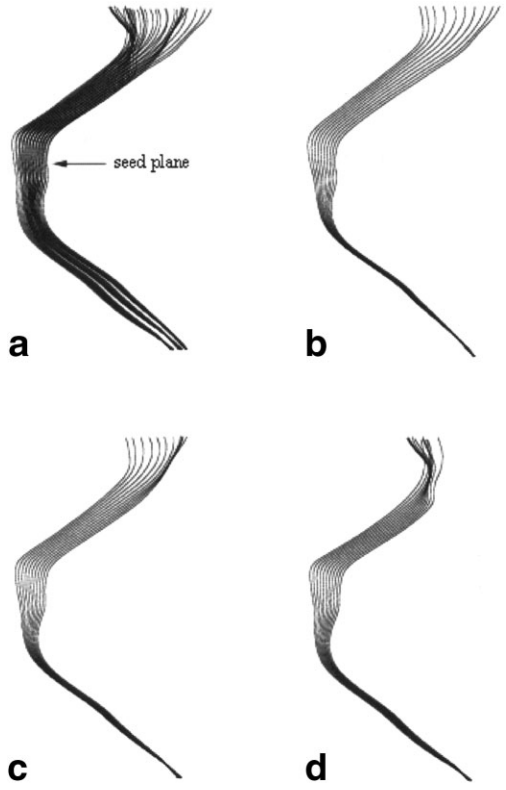


FIG. 8. **a:** The set of fiber pathways shown in Fig. 7. **b–d:** Three fiber bundles obtained from **a** with the bundling algorithm (T = 0.8, K = 3). These fiber bundles correspond to Fig. 6(b–d), respectively.

ular diffusivities, curvature, and torsion are quantified along the medial axis of each fiber bundle. These measures are averaged over the axial length and compared between corresponding fiber bundles. The results are listed in Table 1. As shown in the table, the mean parallel and perpendicular diffusivities measured from the two experiments are highly reproducible, with mean coefficients of variation being 0.027 and 0.034, respectively. Curvature and torsion are somewhat more variable, having mean coefficients of variation equal to 0.087 and 0.090, respectively.

To further test the reproducibility, two additional healthy subjects were similarly scanned. For each subject, the three largest fiber bundles were analyzed to assess the reproducibility of physical and geometric parameters. The mean coefficients of variation over the three tests were 0.023, 0.037, 0.058, and 0.062 for mean parallel diffusivity, mean perpendicular diffusivity, curvature, and torsion, respectively, and the mean mismatches were 1.02 ± 0.34 mm, 0.71 ± 0.30 mm, and 0.85 ± 0.27 mm for these three fiber bundles, respectively.

## DISCUSSION

This article presents our preliminary results of the quantitative analysis of in vivo neuronal fiber pathways. We have developed a system of algorithms to bundle neuronal pathways reconstructed in vivo using DTI and to quantify physical and geometric properties of fiber bundles. Reliability studies demonstrate that physical and geometric measurements are accurate to better than 10% and mismatch of bundle axis is approximately 1 mm, at least in highly anisotropic structures like those studied here.

The focus of this work is on bundling and quantification of neuronal fiber pathways. This kind of higher-level analysis of reconstructed pathways is critical to the development of DTI tractography into a useful tool for studying disease. As mentioned above, reconstruction of neuronal fiber pathways as a technical problem has been the focus of many recent studies. However, most studies to date visually or manually combined the reconstructed fibers to demonstrate fiber tracking algorithms. Bundling fibers into distinct anatomical structures and quantification of those structures have not been explicitly implemented. To the best of our knowledge, this study represents the first effort to characterize the properties of entire fascicles.

Quantification of physical and geometric properties of in vivo fiber bundles may provide sensitive parameters for assisting in the diagnosis of brain diseases; by following temporal changes in those parameters, the progression of disease may be monitored with a sensitivity greater than is available from more conventional MRI techniques. For example, in hydrocephalus, cerebral-spinal fluid accumulates excessively in the ventricles. This causes increased pressure inside the cranium, which in turn compresses the brain tissue (18). It may be useful to evaluate the mechanical impact of hydrocephalus on brain tissue by examining geometric parameters such as curvature or torsion of neuronal fiber bundles, particularly of those near the enlarged ventricles. Furthermore, quantification of in vivo neuronal fiber pathways can be applied to developmental studies of infant brains. As the infant brain develops, the physical and geometric properties of neuronal fibers evolve; characterization of these properties may provide a measure of the relative rates of maturation of different functional systems.

Table 1
Comparison of Physical and Geometric Parameters Measured From Two Experiments for Three Fiber Bundles Shown in Figs. 6 and 8

| | | Mean diffusivity ($\times 10^{-5}$ mm$^2$/s) | | Curvature (mm$^{-1}$) | Torsion (mm$^{-1}$) |
|---|---|---|---|---|---|
| | | Parallel | Perpendicular | | |
| Bundle b | Experiment 1 | 1.1897 | 0.5625 | 0.0045 | 0.0154 |
| | Experiment 2 | 1.1447 | 0.5188 | 0.0040 | 0.0150 |
| Bundle c | Experiment 1 | 1.1827 | 0.5617 | 0.0041 | 0.0192 |
| | Experiment 2 | 1.1974 | 0.5627 | 0.0047 | 0.0230 |
| Bundle d | Experiment 1 | 1.3172 | 0.6335 | 0.0039 | 0.0241 |
| | Experiment 2 | 1.2367 | 0.5965 | 0.0035 | 0.0285 |
| Mean coefficient of variation | | 0.027 | 0.034 | 0.087 | 0.090 |

It is of clinical interest to characterize the collective properties of anatomically distinct fiber bundles. As disability frequently reflects degeneration of a large number of neuronal fibers, quantifying the properties of a fiber bundle is likely more meaningful and informative than measuring individual fiber paths. In this study, we employed a K most-similar-fibers algorithm to bundle fibers. It is a simple yet robust approach to the bundling problem. Although the effectiveness of this algorithm is regulated by a number of parameters, which include the coefficient C, similarity threshold T, and number of most-similar-fibers K, it is not sensitive to the precise values chosen for these parameters. Stable bundling results can be obtained with relatively large range of parameter values. In our implementation, their values are chosen such that a set of fibers is grouped into finer or smaller fiber bundles. This leaves open the option to combine bundles of interest for quantitative characterization.

The concept of a corresponding segment is loosely defined in this study. A precise definition may involve optimization of certain measures between fibers and is beyond the scope of this study. We simply assume that seed points of two fibers to be compared correspond to each other, and determine the corresponding segment by searching along both directions from the seed points. As only neighboring fibers are compared in the bundling algorithm, this approach has proven adequate.

In quantification of neuronal fiber pathways, reproducibility issues exist in diffusion data acquisition, fiber pathway reconstruction, and fiber property characterization. Reproducible diffusion data acquisition is the basis for reliable fiber pathway reconstruction, which in turn is the prerequisite for reproducible characterization of fiber properties. As the focus of this study is on the bundling and quantification of reconstructed pathways, our interest is in examining whether reproducible bundling and quantification results can be obtained from similar sets of diffusion tensor data. This was performed by using interleaved datasets acquired from the same subject, as described above. Testing reproducibility with this approach minimized compounding factors due to diffusion data acquisition and fiber reconstruction.

In this study, typically 7–10 large fiber bundles were found to pass through the right internal capsule, among which the largest three bundles were analyzed for each subject to test reproducibility due to their easier determination of correspondence. The set of large fiber bundles splays toward the cerebral cortex, a phenomenon grossly consistent with anatomical evidence. To validate these results as well as fiber bundles reconstructed in other regions with rigorous anatomical verification, we are planning to carry out animal experiments in which tracer molecules are to be used to track fiber bundles.

It should be pointed out that, although a simple path-following method is employed to reconstruct neuronal fiber pathways in this study, our algorithm for fiber bundling is independent of any particular fiber tracking algorithm used. Nevertheless, a robust fiber-tracking algorithm is always desirable, as it provides a reliable basis for further processing of reconstructed fibers such as fiber bundling. Pitfalls of the simple path-following method include susceptibility to noise and partial volume effects. Evidently, these will limit its capability to reconstruct reliable fiber pathways from noisy diffusion tensor data and handle situations such as fiber bifurcation and crossing (which may be the cause of mismatches between fiber bundles shown in Figs. 6 and 8). These problems have been recently coped with by tracking fiber pathways in a continuous diffusion tensor field constructed from discrete, noisy diffusion data (19), or imposing regularization rules on fiber track directions (20). We expect the bundling algorithm described here will perform even better using pathways calculated with these more sophisticated approaches, and consider incorporating such approaches in our future studies.

## REFERENCES


1. Basser PJ, Mattiello J, LeBihan D. MR diffusion tensor spectroscopy and imaging. Biophys J 1994;66:259–267.
2. Basser PJ, Pierpaoli C. Microstructural and physiological features of tissues elucidated by quantitative-diffusion-tensor MRI. J Magn Reson 1996;111:209–219.
3. Hsu EW, Mori S. Analytical expression for the NMR apparent diffusion coefficients in an anisotropic system and a simplified method for determining fiber orientation. Magn Reson Med 1995;34:194–200.
4. Pierpaoli C, Jezzard P, Basser PJ, Barnett A. Diffusion tensor MR imaging of the human brain. Radiology 1996;201:637–648.
5. Conturo TE, McKinstry RC, Akbudak E, Robinson BH. Encoding of anisotropic diffusion with tetrahedral gradients: a general mathematical diffusion formalism and experimental results. Magn Reson Med 1996;35:399–412.
6. Ulug AM, Bakht O, Bryan RN, van Zijl PCM. Mapping of human brain fibers using diffusion tensor imaging. In: Proc 4th Annual Meeting ISMRM, New York, 1996. p 1325.
7. Jones DK, Simmons A, Williams SCR, Horsfield MA. Non-invasive assessment of structural connectivity in white matter by diffusion tensor MRI. In: Proc 6th Annual Meeting ISMRM, Sydney, 1998. p 531.
8. Mori S, Crain BJ, Chacko VP, van Zijl PCM. Three-dimensional tracking of axonal projections in the brain by magnetic resonance imaging. Ann Neurol 1999;45:265–269.
9. Conturo TE, Lori NF, Cull TS, Akbudak E, Snyder AZ, Shimony JS, McKinstry RC, Burton H, Raichle ME. Tracking neuronal fiber pathways in the living human brain. Proc Natl Acad Sci USA 1999;96:10422–10427.
10. Xue R, van Zijl PCM, Crain BJ, Solaiyappan M, Mori S. In vivo three-dimensional reconstruction of rat brain axonal projections by diffusion tensor imaging. Magn Reson Med 1999;42:1123–1127.
11. Parker GJM. Tracing fibre tracks using fast marching. In: Proc 8th Annual Meeting ISMRM, Denver, 2000. p 85.
12. Moseley ME, Cohen Y, Kucharczyk J, Mintorovitch J, Asgari HS, Wendland MF, Tsuruda J, Norman D. Diffusion-weighted MR imaging of anisotropic water diffusion in cat central nervous system. Radiology 1990;176:439–445.
13. Stejskal EO, Tanner JE. Spin diffusion measurements; spin echoes in the presence of time-dependent field gradient. J Chem Phys 1965;42:288–292.
14. Anderberg MR. Cluster analysis for applications. New York: Academic Press; 1973.
15. Gowda KC, Krishna G. Agglomerative clustering using the concept of mutual nearest neighborhood. Pattern Recogn 1978;10:105–112.
16. Ding Z, Friedman MH. Dynamics of coronary arterial motion and its potential role in coronary atherogenesis. J Biomech Eng 2000;122:488–492.
17. Yuan QS. Fundamentals of computational geometric modeling. Beijing: Aviation Industry Press; 1987.
18. Chou SY, Digre KB. Neuro-ophthalmic complications of raised intracranial pressure, hydrocephalus, and shunt malfunction. Neurosurg Clin N Am 1999;10:587–608.
19. Basser PJ, Pajevic S, Pierpaoli C, Duda J, Aldroubi A. In vivo fiber tractography using DT-MRI Data. Magn Reson Med 2000;44:625–632.
20. Poupon C, Clark CA, Frouin V, Regis J, Bloch I, LeBihan D, Mangin JF. Regularization of diffusion-based direction maps for the tracking of brain white matter fascicles. NeuroImage 2000;12:184–195.